npj | climate and atmospheric science

Article

Published in partnership with CECCR at King Abdulaziz University

https://doi.org/10.1038/s41612-025-00962-9

# ENSO's impact on linear and nonlinear predictability of Antarctic sea ice



Yunhe Wang[1], Xiaojun Yuan[2] ✉, Yibin Ren[1], Xiaofeng Li[1] ✉ & Arnold L. Gordon[2]

While the influence of ENSO on Antarctic sea ice variability is well-known, its role in sea ice predictability, both linear and nonlinear, remains unexplored. This study utilizes deep learning models to quantify ENSO's impact on Antarctic sea ice predictability. We find that ENSO events exert cross-timescale influences on sea ice's subseasonal linear and nonlinear predictability. Within a 3-week lead time, ice persistence is the primary source of predictability. Beyond this period, ENSO becomes a key source of Antarctic sea ice predictability, with El Niño enhancing ice linear predictability more than La Niña. Specifically, El Niño improves ice linear predictability by 25.6%, 19.6%, and 30.4% in the A-B Sea, Ross Sea, and Indian Ocean, respectively, at an 8-week lead time. La Niña mainly enhances ice nonlinear predictability, particularly in the Ross Sea. We demonstrate that ENSO provides additional sources for Antarctic sea ice predictability primarily through generating more extensive ice anomalies. These insights deepen our understanding of sea ice predictability and are crucial for advancing forecasting models.

Despite a gradual increase spanning over three decades[1], with the September Antarctic sea ice extent (SIE) reaching a record high in 2014[2], there was a shift to a dramatic decline in 2015/2016[3–5]. By the summer of 2023, the monthly SIE plummeted to a historical low of 1.91 million square kilometers according to SIE index data from National Snow and Ice Data Center (NSIDC)[6]. This dramatic shift, coupled with large year-to-year variability observed since the mid-1990s[6], underscores the heightened state of variability in the atmosphere-ocean-sea ice system in the Antarctic[2,7]. Accurate sea ice predictions are essential, given the increasing polar activities related to navigation, planning, and rescue operations. Consequently, improving our understanding of Antarctic sea ice predictability is an urgent and timely scientific challenge.

Potential sea ice predictability, a key concept in our study, refers to the theoretical maximum predictive skill of a sea ice forecast system under ideal conditions[8]. This concept assumes a model that perfectly represents reality and nearly perfect knowledge of the initial state of the atmosphere-sea ice-ocean system. However, not all sea ice variability is predictable, and no forecast models can capture all predictable variance. In our study, sea ice predictability refers to the actual predictive skill of a sea ice forecast system under real-world conditions. It is influenced by many factors, which can be broadly categorized into internal variability, external forcings, and observational and modeling constraints. Additionally, sea ice predictability encompasses linear and nonlinear aspects, which have not been explicitly evaluated due to the limitations of traditional statistical and dynamic models. Consequently, this area remains a subject of ambiguity. Linear processes are characterized by straightforward cause-and-effect relationships, where changes in one variable lead to proportional changes in sea ice, such as ice growth in fall driven by surface heat loss. On the other hand, nonlinear processes involve complex interactions and feedback loops, such as ice growth triggered by heat loss, which initiates entrainment at the base of the mixed layer, bringing heat stored in the thermocline into the mixed layer and leading to ice melt.

El Niño-Southern Oscillation (ENSO), renowned as the most substantial interannual variability signal on Earth, exerts a pronounced remote influence on the Antarctic climate system through atmospheric teleconnection[9,10], changing various components of surface climate, including the atmosphere, ocean, sea ice, and glacial ice[11–14]. The teleconnection between ENSO and Antarctic sea ice anomalies is well documented[12,15–17]. During the warm phase of ENSO, sea ice shows negative anomalies in the Amundsen Sea and positive anomalies in the Weddell Sea, and vice versa[17]. ENSO events can influence Antarctic regional atmospheric circulation through two main mechanisms: triggering a southeastward-propagating Rossby wave train and altering the mean meridional circulation of the Hadley Cell and Ferrel Cell[17,18]. These two processes work in phases, significantly increasing sea ice variability in the West Antarctic. The interannual ENSO variability, with its warm and cold phases, can be regarded as different background mean climate states for sea ice variability at a subseasonal timescale. Therefore, we can use ENSO events to assess the mean

[1]Key Laboratory of Ocean Observation and Forecasting and Key Laboratory of Ocean Circulation and Waves, Institute of Oceanology, Chinese Academy of Sciences, Qingdao, China. [2]Lamont-Doherty Earth Observatory of Columbia University, New York, NY, USA. ✉e-mail: xyuan@ldeo.columbia.edu; lixf@qdio.ac.cn

state's impact on sea ice subseasonal predictability. This study aims to answer the following scientific question: Can the influence of ENSO on Antarctic sea ice variability provide additional sources of subseasonal sea ice predictability? Do ENSO events affect sea ice predictability through linear or nonlinear processes in the polar climate system?

A well-constructed model is the foundation for evaluating sea ice predictability. Recent advances in Antarctic sea ice prediction have significantly improved our understanding of sea ice predictability. For example, Bushuk et al.[19] evaluated seasonal prediction skills using three coupled dynamical systems, FLOR, SPEAR_LO, and SPEAR_MED. Morioka et al.[20] investigated the impact of sea-ice initialization on interannual climate predictability over the Weddell Sea. Sea ice predictability is influenced by local factors such as upper ocean heat content (OHC)[19,21,22], upper ocean vertical structure[23], sea ice thickness (SIT)[24,25], and decadal variability in tropical Pacific sea surface temperature (SST)[26,27], which has been documented. However, dynamical models still face substantial limitations due to insufficient observations and gaps in understanding key physical mechanisms[5,28,29]. SIE forecasts within the Sea Ice Prediction Network South (SIPN South) reveal a larger spread in dynamical models than observed uncertainties and still need to be more accurate to guide field planning or maritime route forecasting[30,31]. Similarly, the Coupled Model Intercomparison Project Phase 6 (CMIP6) models still encounter difficulties in capturing pre-2014 trends and displaying broad intermodel variability[29,32,33]. Advanced statistical models, such as linear Markov models[17,34], are designed to capture co-variability in the atmosphere-ocean-sea ice system but face limitations in representing nonlinear processes and spatiotemporal synchronized evolution.

Nevertheless, deep learning models, characterized by their multilayered neural network structures, can learn and depict intricate nonlinear relationships within the data. It opens up an alternative approach to predicting Antarctic sea ice, proving to significantly surpass the predictive capabilities of the Markov model and current state-of-art dynamical models, such as ECMWF, NCEP, and GFDL-SPEAR, at the subseasonal timescale[35]. Additionally, it can separately evaluate sea ice's linear and nonlinear predictability, assisting us to explore sources of sea ice predictability in more profound steps. Here, we employ a deep learning model: sea ice prediction network (SIPNet, see "Methods") to identify the effects of different ENSO phases on Antarctic sea ice's subseasonal linear and nonlinear predictability. Answers to these scientific questions can improve understanding of the Antarctic coupled climate system, and are vital for advancing our ability to predict Antarctic sea ice, aiding societal response to climate change challenges.

## Results

### SIPNet skill from linear and nonlinear processes

Complicated atmosphere-ocean-sea ice interactive processes drive Antarctic sea ice concentration (SIC) variability. SIPNet allows us to examine these processes from a data-driven point of view without explicitly describing individual physical processes. We first examine where SIPNet exhibits significant skill measured by anomaly correlation coefficient (ACC) at the subseasonal timescale as a function of regions. The Antarctic is subdivided into five subregions based on NSIDC classifications (Supplementary Fig. 2). Based on the deviation degree between the ACC histograms (see "Methods") of the SIPNet and the anomaly persistence, the results were categorized into two groups: ACC distribution for 1–3- and 4–6-week leads. At 1–3-week leads, SIPNet model skill and anomaly persistence showed relatively similar distributions with ACC peaks close to 0.85 (Fig. 1a). SIPNet demonstrates overall higher ACCs. The two peaks in the ACC histograms of the persistence forecast are likely due to high-frequency variability in the marginal ice zone, low-frequency variability in the inner ice zone, and the zonal asymmetry of Antarctic sea ice variability. On the other hand, at 4–6-week leads, the anomaly persistence ACCs significantly shifted to lower values with distribution modes at 0.4 or less. In contrast, SIPNet's mode remains 0.6–0.8 (Fig. 1b), suggesting that the model progressively captures more predictable variance beyond sea ice persistence with extended lead times.

Then, we focus on the SIC predictions at 4–6 week lead times and further isolate the sources of SIPNet's skill. A linear SIPNet was developed by deactivating all nonlinear activation functions in SIPNet. Consequently, the nonlinear SIPNet skill can be calculated by subtracting the linear SIPNet skill from the total SIPNet skill. To compare the spatial distribution of linear and nonlinear model skill, we averaged those skill over 4–6 weeks lead predictions. The overall pattern of linear SIPNet skill resembles anomaly persistence skill but with slightly elevated values in the Weddell Gyre and east of the Ross Sea (Fig. 2b, d). The higher skill of linear SIPNet is concentrated in outer ice pack regions and Antarctic Dipole (ADP) regions,

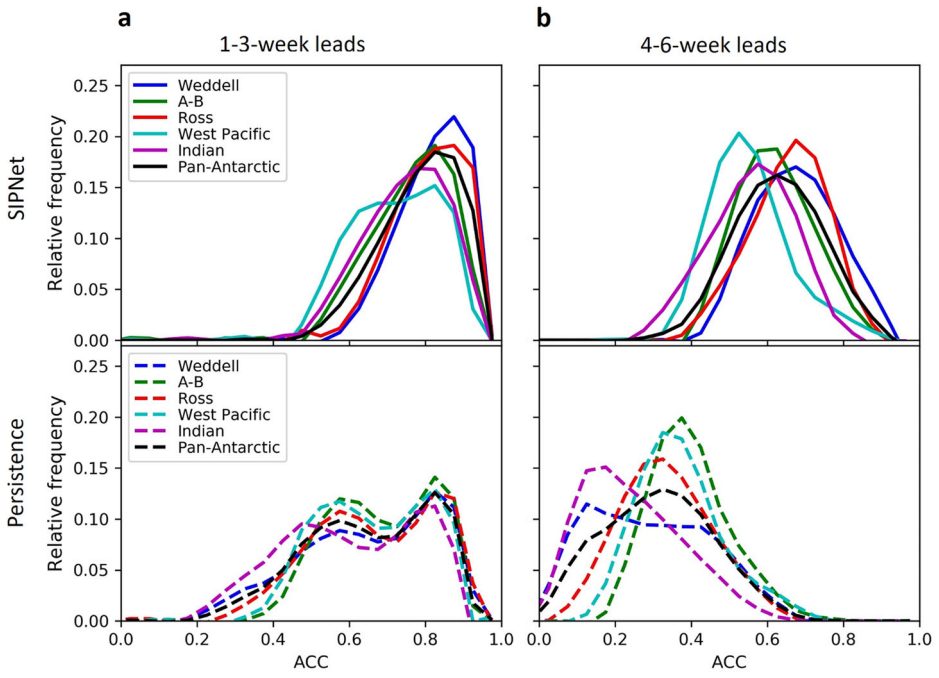


**Fig. 1 | Distributions of model skill of SIPNet and anomaly persistence with increasing lead time.** **a** Regional ACC histogram from SIPNet and anomaly persistence at 1–3-week leads. **b** Same as (**a**) but for 4–6 week leads. The Kolmogorov–Smirnov (KS) test $p$ values for comparing the ACC distributions of the SIPNet model and the anomaly persistence across all Antarctic regions and two lead time groups are all 0, indicating that the ACC distributions between the two models are statistically significantly different in each region, respectively.

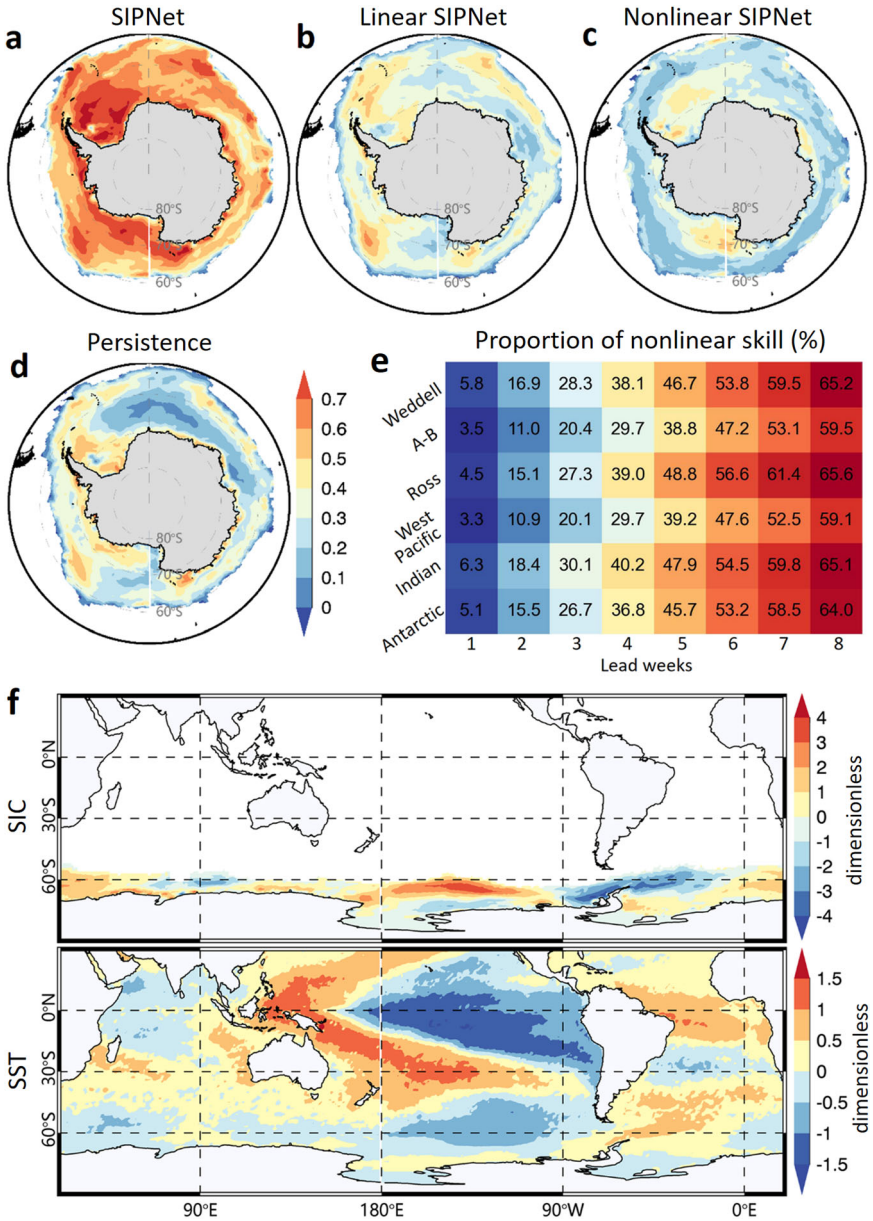


**Fig. 2 | Mean model skill, measured by ACC between SIC observation and prediction anomalies at 4–6 week leads and spatial patterns of the first SVD mode between SIC and SST. a** SIPNet skill. **b** Linear SIPNet skill. **c** Nonlinear SIPNet skill, determined by subtracting the linear SIPNet skill (**b**) from the total SIPNet skill (**a**). **d** Anomaly persistence skill. **e** The proportion of nonlinear SIPNet skill relative to the total SIPNet skill for each region across lead times of 1–8 weeks. **f** Spatial patterns of the first SVD mode between weekly SIC and SST, where the mode accounts for 52% of total covariance, with a correlation coefficient of 0.67 between the SIC and SST modes time series of the leading mode.

which refer to the Amundsen Sea and Weddell Sea[14]. In contrast, the higher nonlinear skill is predominantly observed in inner ice pack regions of the Weddell and Ross Gyres, mainly during summer and autumn (not shown). In general, nonlinear processes provide an additional 0.1–0.4 skill to the SIPNet linear skill at 4–6 week lead forecasts. Furthermore, we computed the ratio of nonlinear skill to total SIPNet skill for 1–8 week lead forecasts individually (Fig. 2e). The results show that this proportion rises with an increase of lead time across all Antarctic regions, suggesting that nonlinear processes growth progressively within the atmosphere-ocean-sea ice system. Beyond the 6-week lead, the nonlinear skill emerges as the predominant contributor to SIPNet skill.

Additionally, we applied another approach to calculate the nonlinear SIPNet skill by computing the ACC between observations and nonlinear SIC predictions, which are obtained by subtracting linear SIPNet SIC predictions from total SIPNet SIC predictions. The results of this method are largely consistent with the above conclusions, despite some regional differences (Supplementary Fig. 3). For instance, higher nonlinear skill is predominantly observed in the inner ice pack regions of the Weddell and Ross Gyres. Moreover, the proportion of this nonlinear SIPNet skill increases with longer lead times across all Antarctic regions from both methods. This demonstrates that our method of deriving nonlinear SIPNet skill by subtracting the linear SIPNet skill from the total SIPNet skill is effective. In the following sections, we will primarily adopt this approach.

Previous studies suggest that Antarctic sea ice is influenced by remote climate signals, such as the Pacific Decadal Oscillation (PDO), Atlantic Multidecadal Oscillation (AMO), Madden-Julian Oscillation (MJO), and southern mid to high-latitude climate modes like the Southern Annular Mode (SAM) and wave-3 pattern at different time scales[12,36–40]. Specifically, the PDO and AMO represent decadal to multidecadal oscillations whose impact on Antarctic sea ice does not exhibit significant differences across different ENSO phases. The MJO, characterized as a tropical intraseasonal oscillation with eastward movement[41], exerts much less influence on Antarctic sea ice than ENSO events, which significantly impact the sea ice through the generation of a stationary Rossby wave. SAM, the principal climate mode in the Southern Hemisphere, shows peak variability at the subseasonal scale. Its impact on Antarctic sea ice varies with zonal symmetry: in a zonally symmetric state, it has weaker effects due to the lack of strong meridional anomalies, while in a zonally asymmetric state, its interaction with ENSO leads to a more significant influence on sea ice in the ADP region[42,43]. The impact of wave-3 is also enhanced by ENSO in the ADP

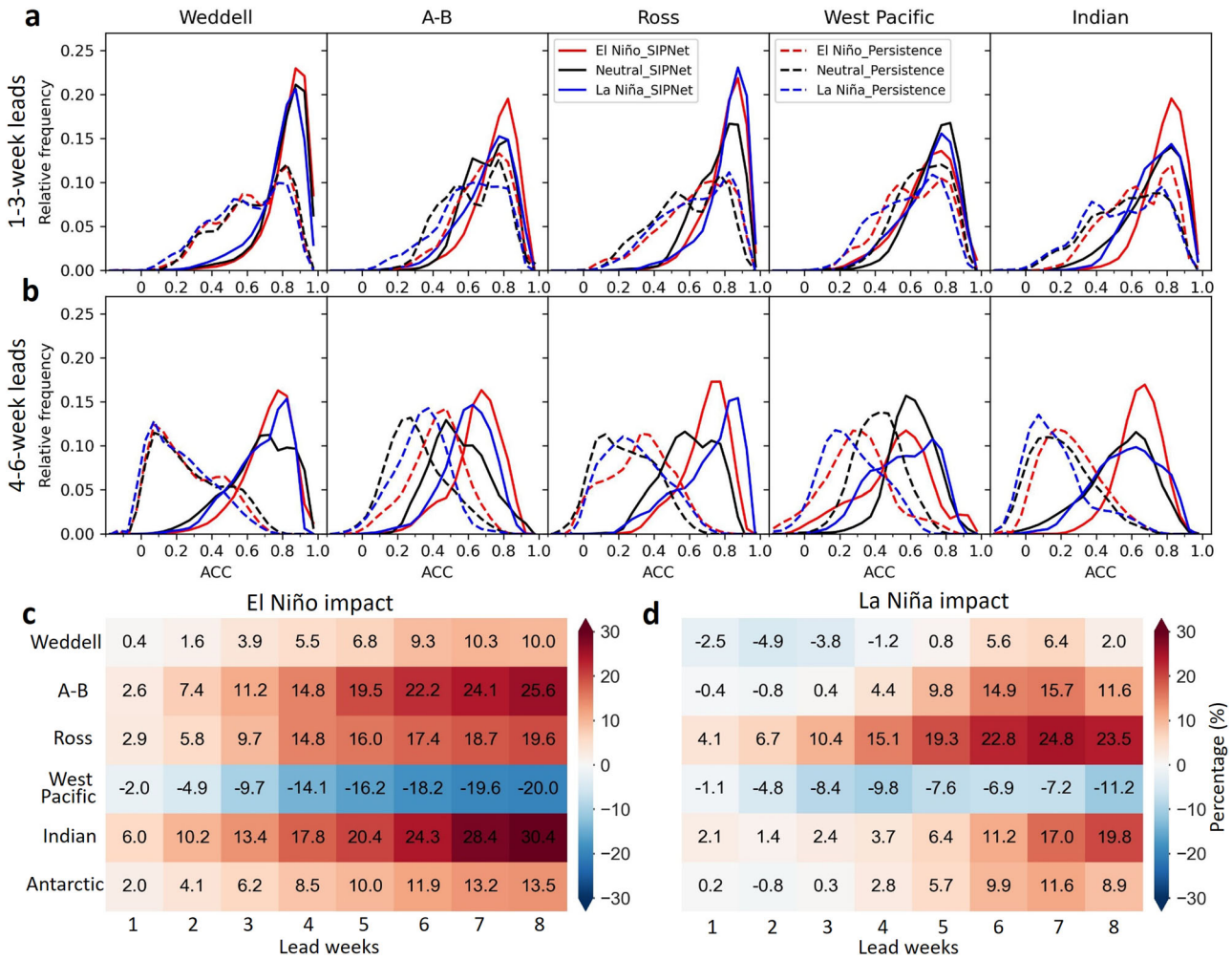


**Fig. 3 | Regional model skill under different ENSO phases. a** ACC histograms from SIPNet predictions and anomaly persistence under different ENSO phases at 1–3-week leads. **b** Same as (**a**) but for 4–6 week leads. **c** The impact of El Niño on SIPNet skill, calculated as the difference between SIPNet skill under El Niño and neutral conditions, divided by the SIPNet skill under neutral conditions. **d** Same as (**c**) but for La Niña. The KS test *p* values are all 0 for ACC distribution comparisons between SIPNet model and anomaly persistence across Antarctic regions, ENSO phases, and lead time groups, indicating that the ACC distributions between the two models are statistically significant different in each region, respectively.

region, despite being a circumpolar phenomenon[42]. Consequently, large sea ice anomalies in the ADP region are mainly influenced by ENSO teleconnections and the interaction between ENSO and the Antarctic climate modes.

To assess whether the interannual variability signal of ENSO exerts a significant influence on Antarctic sea ice at the subseasonal scale, we further analyzed the relationship between weekly Antarctic SIC and global SST using singular value decomposition (SVD). The analysis reveals that the first SVD mode accounts for 52% of the total covariance. The SST spatial pattern of this mode strongly corresponds to ENSO, and its temporal coefficients are highly correlated (0.67) with the first SIC mode (Fig. 2f). The SST spatial pattern of the second SVD mode does not exhibit distinctive climatic characteristics (Supplementary Fig. 4a). The explained covariance of the remaining modes is relatively low, all below 10% (Supplementary Fig. 4b). This underscores the dominant influence of ENSO-induced surface climate anomalies on Antarctic sea ice subseasonal variability. Hence, examining how ENSO warm and cold phases impact the subseasonal predictability of sea ice holds considerable scientific significance.

### Quantifying ENSO's impact on SIC predictability

We examined the ACC histograms across three distinct ENSO phases: El Niño, La Niña, and neutral conditions, as delineated in the "Methods" section. The results indicate that at 1–3 week lead times, the ACC distributions of SIPNet slightly shift toward higher values compared with persistence predictions across different ENSO phases in all regions (Fig. 3a), indicating that sea ice predictability primarily relies on ice persistence, with insignificant impact from ENSO. However, anomaly persistence significantly reduces at 4–6 week leads (shifts to the left) while the SIPNet continuously captures predictable variance, resulting in two well-separated skill distribution modes between persistence and SIPNet predictions. Although ENSO (an external factor) enhanced sea ice persistence, it could not offset the decline in the component of SIC persistence related to ice intrinsic variability. Moreover, SIPNet skill notably varies across different ENSO phases (Fig. 3b). Both El Niño and La Niña enhance sea ice predictability in the Amundsen and Bellingshuasen Seas (A-B) and Ross Seas. El Niño amplifies predictability in the Indian Ocean, whereas La Niña's impact is insignificant. In contrast, ENSO events exhibit a diminishing effect on sea ice predictability in the West Pacific. The Weddell Sea demonstrates higher skill during ENSO events than in neutral conditions. However, this enhancement is insignificant, indicating that the Weddell Sea may possess other crucial sources of sea ice predictability under neutral conditions.

Figure 3c, d shows a quantitative analysis of the ENSO's impact on SIPNet skill across 1–8 weeks lead times. El Niño negatively affects sea ice prediction skill in the West Pacific, intensifying from −2% at a 1-week lead to −20% at an 8-week lead (Fig. 3c). Conversely, El Niño enhances sea ice predictability in other Antarctic regions, with the most positive impact in the

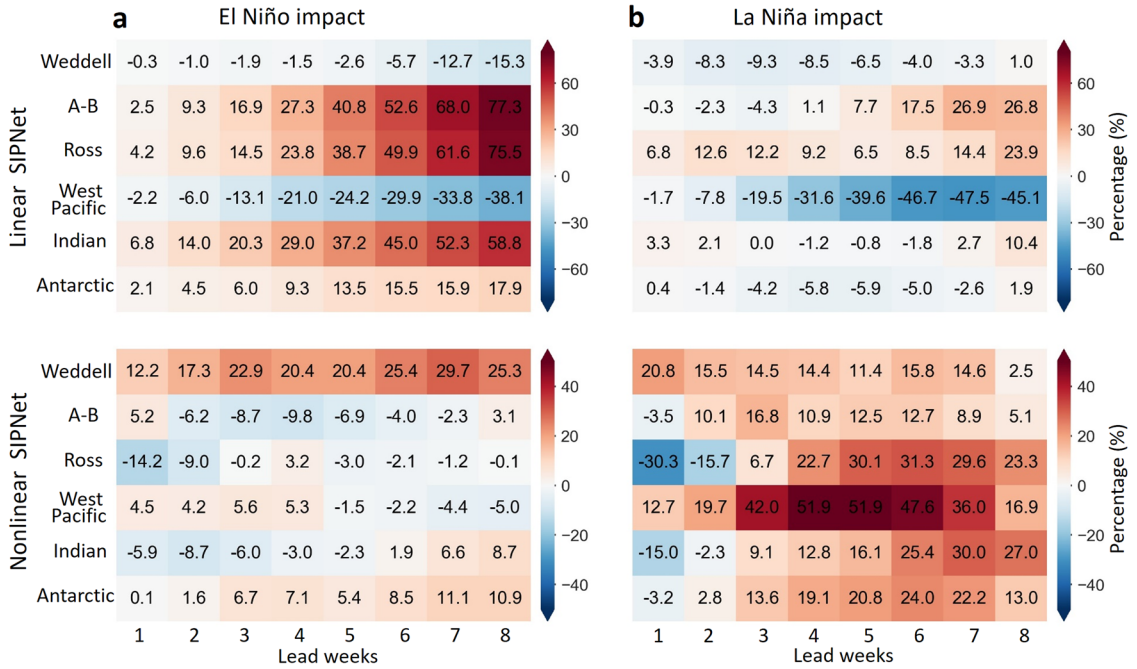


**Fig. 4 | Contribution of different ENSO events to linear and nonlinear SIPNet skill. a** Contribution of El Niño on linear SIPNet skill, calculated as the difference between linear SIPNet skill under El Niño and neutral conditions, divided by the linear SIPNet skill under neutral conditions. The impact of El Niño on nonlinear SIPNet skill is calculated using a similar methodology. **b** Same as (**a**) but for La Niña.

Indian Ocean and A-B Sea, respectively, 30.4% and 25.6% improvement at 8-week leads. Overall, El Niño enhances sea ice predictability in the Pan-Antarctic. On the other hand, La Niña demonstrates a similar pattern of influence on sea ice predictability, albeit weaker (Fig. 3d). It improves prediction skill in the Ross Sea by 23.5% at an 8-week lead, but diminishes skill in the West Pacific across all lead times. La Niña also improves sea ice predictability for the Pan-Antarctic, especially at 6–8 weeks lead times. However, the contribution of different ENSO events to SIPNet skill, whether mainly through affecting the linear or nonlinear sea ice predictability, requires further investigation.

### ENSO-related linear and nonlinear SIC predictability

We quantitatively analyzed the effect of ENSO events through linear and nonlinear SIPNet skill across all lead times. The results indicate substantial differences in the impact of different ENSO phases on both linear and nonlinear SIPNet skill (Fig. 4). El Niño significantly enhances linear ice predictability in the A-B Seas, Ross Sea, and the Indian Ocean, contributing 77.3%, 75.5%, and 58.8% improvement, respectively, at an 8-week lead time (Fig. 4a). In the Weddell Sea, El Niño mainly contributes to the nonlinear ice predictability. Conversely, El Niño predominantly decreases the linear ice predictability in the West Pacific, with a reduction of 38.1% at an 8-week lead time. Overall, El Niño contributes to both linear and nonlinear ice predictability across all lead times in the Pan-Antarctic region, with a greater impact on linear ice predictability. Another approach, which calculates the ACC from nonlinear SIC predictions obtained by subtracting linear SIPNet SIC predictions from total SIPNet SIC predictions, also confirms that La Niña primarily enhances nonlinear ice predictability, contributing up to approximately 20% to Pan-Antarctic SIC predictability within an 8-week lead time (not shown).

On the other hand, La Niña contributes significantly more to the nonlinear ice predictability in nearly all regions, especially at lead times of 3–8 weeks (Fig. 4b). For instance, in the Indian Ocean and Ross Sea, La Niña contributes 30% and 29.6% of improvements to the nonlinear skill, respectively, at a 7-week lead time. Although La Niña significantly enhances the nonlinear model skill in the West Pacific, it also notably decreases the linear model skill, resulting in an overall reduction in the total SPINet skill. Additionally, both El Niño and La Niña increase the nonlinear model skill and decrease the linear model skill in the Weddell Sea. Overall, El Niño primarily enhances the linear ice predictability for the Pan-Antarctic, while La Niña enhances the nonlinear ice predictability. In addition, the representation of Antarctic sea ice linear predictability derived from the linear Markov model closely aligns with the results of the linear SIPNet (Supplementary Fig. 5), indicating a consistent influence of ENSO events on linear predictability across different regions, despite some regional differences. This demonstrates the feasibility of capturing and forecasting the linear processes in sea ice by deactivating the nonlinear activation functions of AI models.

To further examine whether the phenomenon of El Niño contributing more to linear ice processes and La Niña contributing more to nonlinear processes is also reflected in observations, we conducted a linear and nonlinear analysis of observed sea ice variability. The ACC of SIC anomaly persistence presented in Fig. 3b not only serves as a baseline for model skill assessment but also effectively reflects the linear process in sea ice because the ACC reflects the linear correlation between the initial and target sea ice anomaly series. The square of the ACC is equivalent to the proportion of total variance of two ice anomaly series explained by this linear process. In Fig. 3b, the red and blue dashed curves of the histogram show significant rightward shift compared to the black dashed curves in the A-B Sea, Ross Sea, and Indian Ocean. The shift of red curves is greater than the blue curves, indicating that El Niño events induce more linear responses of sea ice than La Niña in observations. SIPNet skill properly reflects these characteristics in observations.

However, accurately quantifying the nonlinear processes of sea ice variability remains challenging, as there is no definitive boundary between nonlinear signals and noise. Nevertheless, we can provide a simple assessment. Based on the characteristics of the sea ice data, we employed polynomial fitting for the initial and target time in observed SIC fields. We fitted polynomial models of orders 1 to 10 to the sea ice time series at each grid cell and calculated the explained variance. We used the adjusted $R^2$, which corrects for the number of independent variables and sample size, and helps prevent overfitting by penalizing excessive model complexity. We selected the maximum adjusted $R^2$ at each grid point as the final explained variance.

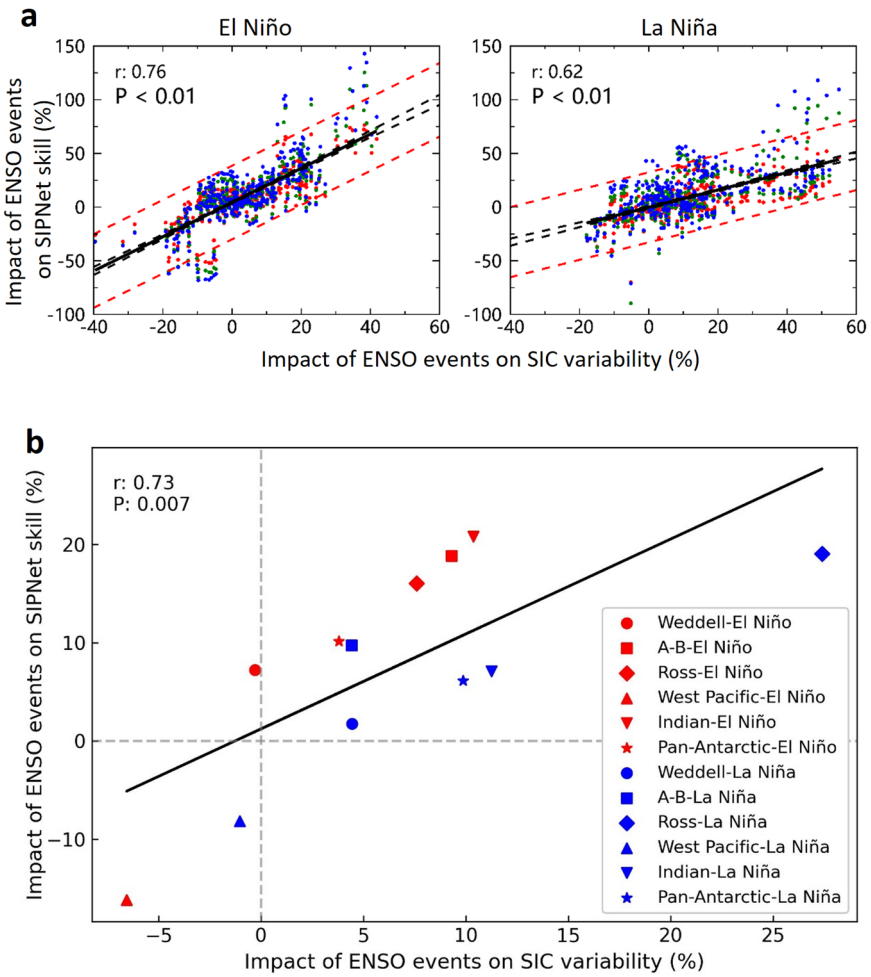


**Fig. 5 | Relationship between SIPNet skill and SIC variability under different ENSO phases.** **a** Scatterplots of the impact of ENSO events on SIPNet skill as a function of the impact of ENSO events on SIC weekly variability within 1° longitude bins. The impact of El Niño (La Niña) on SIPNet skill is computed as the difference between ACC over 4–6-week leads under El Niño (La Niña) and neutral conditions, divided by the latter. The red, green, and blue dots represent the prediction skill corresponding to lead times of 4, 5, and 6 weeks, respectively. Similarly, The impact of El Niño (La Niña) on SIC weekly variability is computed as the difference between SIC weekly standard deviation under El Niño (La Niña) and neutral conditions, divided by the latter. **b** is similar to **a** but shows the regional averages. The solid line represents the linear fit of the data. "r" denotes the correlation coefficient, and "P" denotes the *p* value. "Weddell-El Niño" denotes the impact of El Niño events on sea ice variability and predictability in the Weddell Sea.

The difference between the adjusted $R^2$ and the variance from linear fitting (Supplementary Fig. 6a) reflects the variance attributed to nonlinear processes (Supplementary Fig. 6b), effectively highlighting the spatial distribution of these processes and their relative importance under different ENSO events. We further represented the nonlinear explained variance for each region as histograms, with three curves indicating the distribution of nonlinear explained variance across the three ENSO phases (Supplementary Fig. 6c). The notable rightward shift of the blue dashed curves indicates that La Niña primarily contributes to the nonlinear processes in observed sea ice in all regions, which is captured by the SIPNet (Fig. 4).

### SIPNet skill and SIC variability across ENSO phases

The results above confirm that ENSO events have a significant cross-timescale impact on the subseasonal predictability of Antarctic sea ice. But how do ENSO events influence Antarctic sea ice subseasonal predictability? We first examined relationships between the model skill (measured by the average ACC over 4–6 week leads) and sea ice variability across all Antarctic regions. The results show that model skill and sea ice variability are somewhat linearly related in most regions, suggesting that greater sea ice variability leads to higher predictability, and vice versa, at the subseasonal timescale (Supplementary Fig. 7). The correlations reach 0.57 and 0.60 in the A-B and Ross Seas, respectively, while the correlation in the Pan-Antarctic remains at 0.44.

Additionally, previous studies have shown that ENSO significantly impacts Antarctic sea ice variability[11–14]. Naturally, we raise the question: Does ENSO influence sea ice predictability by generating more high sea ice variability? We calculated the weekly variability of Antarctic sea ice at each grid point under different ENSO phases and compiled sea ice histograms in each region (Supplementary Fig. 8). The results indicate that the ENSO-Antarctic teleconnection has increased sea ice variability in the A-B Sea, Ross Sea, and Indian Ocean, while having little impact on the Weddell Sea. In contrast, it has reduced sea ice variability in the West Pacific, which aligns with ENSO's influence on sea ice predictability (Fig. 3b). To further validate the relationship between ENSO and sea ice predictability, we analyzed the correlation between ENSO-induced sea ice variability and ENSO-induced prediction skill (ACC) within 1° longitude bins around the Antarctic (Fig. 5a). The linear correlation coefficients were 0.76 for El Niño and 0.62 for La Niña, both exceeding the 99% significance level. The primary distribution of points in different colors shows no significant relative shift, indicating that this relationship holds consistently across lead times. It is worth noting that the green and blue dots slightly deviate from the linear relationship at higher sea ice variability, partially indicating a nonlinear component in this relationship. It confirms that ENSO positively influences sea ice predictability by generating larger ice anomalies. Compared to La Niña, El Niño enhances sea ice predictability more significantly by increasing sea ice variability through linear processes (Fig. 5a, b).

Figure 5a only reflects the overall situation across the entire Antarctic and cannot capture the specific relationship between ENSO-induced sea ice variability and ENSO-induced prediction skill in individual regions. We calculated the average of both in each region and then presented their relationship. The results show a correlation coefficient of 0.7 between them, exceeding the 99% confidence level (Fig. 5b). La Niña/El Niño provides additional sources for sea ice predictability in the Ross Sea, A-B Sea, and the Indian Ocean by generating larger and more persisting sea ice anomalies, while limiting the predictability in the Western Pacific by reducing sea ice variability and persistence (Figs. 3b and 5).

After confirming the relationship between ENSO, sea ice variability, and predictability, we attempt to clarify the physical processes through which ENSO influences sea ice predictability. Using Rossby waves as an example, we conducted composites of weekly SST, surface air temperature (SAT), sea level pressure (SLP), observed SIC, and predicted SIC anomalies during different ENSO phases. Supplementary Fig. 9 illustrates the influence process of La Niña on Antarctic sea ice predictability. La Niña events reach maturity during the austral summer and SST anomalies alter tropical convection, triggering a southeastward-propagating Rossby wave train and creating a cold-phase Pacific South American (PSA) pattern in autumn. In response to the PSA pattern, a regional circulation tends to transport warm air from lower latitudes to the Weddell/Bellingshausen Seas, while cold Antarctic air is advected to the open ocean via the Ross/Amundsen Seas. This anomalous circulation induces ADP anomalies in the SIC field during winter and spring, with positive anomalies in the Ross/Amundsen Seas and negative anomalies in the Weddell/Bellingshausen Seas. The influence of El Niño on Antarctic sea ice is similar to that of La Niña, but with opposite phase anomalies (Supplementary Fig. 10). This result is consistent with earlier studies[17].

Consequently, the Ross Sea, A-B, and Weddell Seas, including the areas surrounding the Antarctic Peninsula, are significantly influenced by ENSO teleconnections. During ENSO events, sea ice anomalies in these regions increase, leading to more predictable variance that models can easily capture, enhancing sea ice predictability (Fig. 3). The Weddell Sea, governed by the Weddell Gyre constrained by its western boundary, the Antarctic Peninsula, and the Antarctic Circumpolar Current (ACC), supports a stable, large-scale clockwise sea ice advection. This creates a consistent sea ice variability signal that models can effectively capture, thereby enhancing predictability even in the absence of ENSO forcing. The Ross Gyre, with a limited western boundary and greater distance from the ACC, lacks sufficient stability in sea ice advection to significantly improve ice predictability without ENSO influence. In the Indian Ocean, high sea ice predictability during El Niño events can be attributed to a low-pressure anomaly extending from the South Atlantic into the Indian Ocean during June to August of ENSO mature years (Supplementary Figs. 9 and 10), accompanied by onshore winds that cause widespread warming and negative sea ice anomalies, providing models with more variability signals. In contrast, the West Pacific experiences weaker atmospheric circulation during El Niño (Supplementary Figs. 10 and 11), leading to less pronounced sea ice anomalies and making it challenging for models to predict sea ice variability. However, from March to August in neutral years, enhanced circulation anomalies in the West Pacific significantly improve sea ice anomaly signals and predictability.

## Discussion

Our analysis exclusively focused on the Nino3.4 index to assess the impact of different ENSO phases on Antarctic sea ice predictability. However, ENSO events exhibit considerable diversity in terms of amplitude, temporal evolution, and spatial SST anomaly patterns (Supplementary Fig. 12). These variations influence the teleconnections to Antarctic climate variability[16,44–46], having different effects on sea ice predictability. Compared with EP El Niño, CP El Niño tends to produce a westward-shifting Rossby wave train over the entire South Pacific, leading to a shifted ASL and associated ADP anomalies[12,16,47]. Specifically, the Niño3 index (SST anomaly over 5°S–5°N, 150°W–90°W) primarily reflects eastern Pacific (EP) ENSO, while the Niño4 index (5°S–5°N, 160°E–150°W) focuses on central Pacific (CP) ENSO. The Niño3.4 index (5°S–5°N, 170°W–120°W) represents a combination of both. However, distinguishing between EP and CP ENSO events using the Niño3 and Niño4 indices is challenging due to their high correlation[48].

To better differentiate EP and CP El Niño events, we introduced the $N_{EP}$ and $N_{CP}$ indices in this study, derived from the following Eq. (1)[48]:

$$\begin{cases} N_{EP} = N_3 - \alpha N_4 \\ N_{CP} = N_4 - \alpha N_3 \end{cases}, \quad \alpha = \begin{cases} 0.4, & N_3 N_4 > 0 \\ 0, & \text{otherwise} \end{cases} \tag{1}$$

where $N_3$ and $N_4$ denote the Niño3 and Niño4 indices. Given the limited diversity in La Niña events, our primary focus was on El Niño diversity. An EP El Niño event is identified when the $N_{EP}$ index exceeds one standard deviation for at least four consecutive months from September to March of the following year, while a CP El Niño event is identified by the $N_{CP}$ index meeting this criterion. As a result, four of the eleven El Niño events are classified as EP and five as CP El Niño (Supplementary Fig. 12). For example, the 1982/1983 El Niño is classified as EP, while the 2009/2010 event is classified as CP. Although EP and CP El Niño events introduce anomalous sea ice at different locations, their impacts on the subseasonal predictability of Antarctic sea ice are consistent (Fig. 6). Both contribute positively to sea ice predictability in the A-B Sea, Ross Sea, and Indian Ocean, while reducing predictability in the West Pacific. Although EP and CP contribute to sea ice predictability in the Weddell Sea to some extent, their impact is smaller compared to other regions. Notably, the slight difference between Figs. 3b and 6 may stem from the reduced sample size after classifying El Niño events, which halved the data, and from the ENSO-Antarctic teleconnections occurring in different regions under EP and CP conditions, affecting ACC statistics. However, these factors do not change the conclusion regarding El Niño's impact on sea ice predictability.

Previous studies have shown that the IOD and high-latitude climate modes, such as SAM and the wave-3 pattern, also influence Antarctic sea ice[42,49]. While ENSO shares some variance with these modes on interannual timescales, it is challenging to fully disentangle their specific contributions to sea ice predictability. However, the formation mechanisms of IOD, SAM, and wave-3 are largely independent of ENSO, and their shared variance is less than 9% (Supplementary Fig. 13). Our results indicate that ENSO events influence sea ice predictability primarily through direct teleconnections or interactions with other remote or regional climate modes.

In addition, SIPNet enhances our ability to assess Antarctic sea ice predictability, benefiting from several advantages. It employs an end-to-end modeling approach, where prediction results are obtained directly from input to output, with prediction errors backpropagated through every network layer to optimize parameters. This holistic methodology eliminates the need for compartmentalization into multiple modules, avoiding error accumulation associated with stepwise modeling. Additionally, SIPNet exclusively relies on SIC data for both training and forecasting. Arising from integrated interactions between the atmosphere and ocean, sea ice variability demonstrates strong spatiotemporal interdependencies and a high signal-to-noise ratio. With over ten million parameters, a residual connection, and an encoder-decoder structure, SIPNet enables a deeper exploration of complex relationships within sea ice sequences[35], transforming larger anomaly information into higher skill.

This study examined the subseasonal predictability of Antarctic sea ice changes under the background of different ENSO phases. Using the SIPNet model and a linear SIPNet model, we quantitatively analyzed whether different ENSO events primarily influence sea ice's linear or nonlinear predictability. By examining the evolution of SST, SLP, SAT, observed SIC, and predicted SIC fields under different ENSO events, and analyzing the relationship between sea ice predictability and variability, we discussed the physical processes and mechanisms by which ENSO events affect Antarctic sea ice predictability.

The main findings are as follows: First, the Antarctic sea ice predictability at short lead times (1–3 weeks) is primarily provided by the persistence of sea ice anomalies itself, with insignificant influence from ENSO events. As the lead time increases, the contribution of intrinsic sea ice variability to persistence decreases rapidly, while ENSO's impact on persistence and predictability increases. Nonlinear predictability also becomes significant and dominates beyond a 6-week lead time. Second, ENSO events significantly impact Antarctic sea ice predictability beyond a 3-week lead, with El Niño events having a greater overall impact on ice predictability than La Niña. Specifically, El Niño events mainly affect linear predictability, significantly enhancing overall sea ice predictability in the A-B Sea, Ross Sea, and Indian Ocean by 25.6%, 19.6%, and 30.4%, respectively, at an 8-week lead time. La Niña events primarily enhance nonlinear predictability,

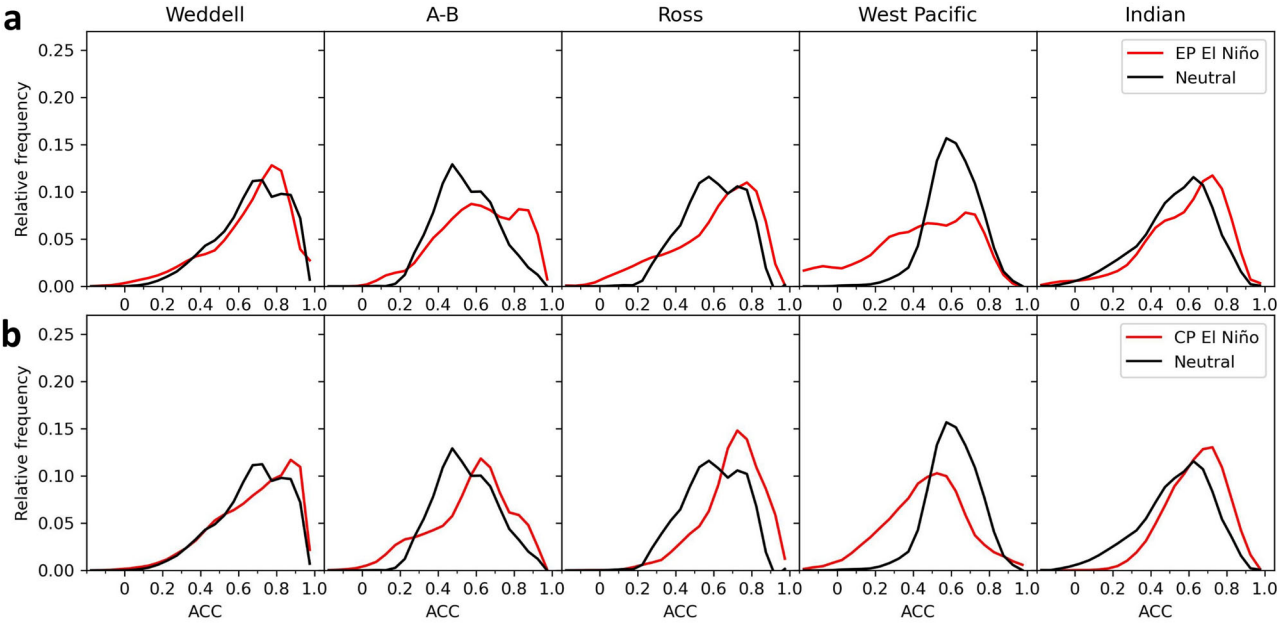


**Fig. 6 | Regional model skill under El Niño and neutral conditions. a** ACC histograms from SIPNet predictions under EP El Niño events (red) and neutral conditions (black) at 4–6 week leads. **b** Same as (**a**) except for CP El Niño.

improving the overall ice predictability in the Ross Sea. However, both events reduce linear predictability, markedly decreasing overall predictability in the West Pacific. Third, ENSO's teleconnections to the Antarctic climate generate larger and more persistent ice anomalies, providing additional predictable variance, which is effectively captured and represented by SIPNet. Additionally, the underlying reasons why La Niña events contribute more to nonlinear ice variability and predictability, while El Niño events predominantly enhance linear variability and predictability, remain unclear and will be explored in future research.

Additionally, due to the current limitations in the interpretability of deep learning models, we acknowledged the need for further understanding of how deep learning transforms high sea ice variability into high skill. We anticipate that ongoing developments in deep learning technology will provide valuable insights into this intriguing research direction. The findings in this study reveal the intricate link between ENSO and Antarctic sea ice subseasonal predictability, offering assistance to scientists, policymakers, environmental groups, and diverse communities in addressing societal needs and climate change challenges in polar regions.

## Methods

### SIPNet model

SIPNet is a deep-learning model driven exclusively by SIC data, designed to predict Antarctic sea ice at the subseasonal time scale[35] (Supplementary Fig. 1a). The SIPNet model features a multi-scale nested encoder-decoder structure, including input, encoder, decoder, and output modules[35].

The model encoder comprises convolutional neural networks (CNNs), best at identifying images such as SIC, and $2 \times 2$ kernel max-pooling layers (green arrows in Supplementary Fig. 1a). These max-pooling layers reduce the size of the feature maps, emphasizing larger-scale spatial information of sea ice while diminishing fine-scale details. The combination of CNN and max-pooling captures spatiotemporal dependencies within the historical SIC sequence. In our model, CNN is embedded in a residual CNN (ResNet) block that involves two stacked CNN layers interconnected by a shortcut linking the first CNN layer's input to the second layer's output[50,51] (Supplementary Fig. 1a). This residual connection facilitates inter-layer connections, prevents signal attenuation, effectively preserves gradient information, and addresses the problem of gradient vanishing as the neural network deepens[52]. The encoder consists of four stages, with each stage containing increasingly lower spatial resolution maps, aiming to capture predictable features with different spatial scales.

Conversely, the decoder employs upsampling and convolutional layers to magnify spatial dimensions while reducing feature maps. The feature maps generated by the decoder feed into the output module. The output module includes a single CNN layer with eight $1 \times 1$ convolutional kernels, applying a sigmoid activation layer to predict SIC in each grid cell. The loss is computed by comparing the predicted and observed SIC. The model achieves a high-performance state by iteratively minimizing losses, and it employs zero padding to maintain consistent spatial dimensions between the input and the output SICs. In addition, based on extensive sensitivity experiments conducted earlier, the SIPNet model is configured with a learning rate of 0.0001, filter sizes of $3 \times 3$, and a batch size of 8. We also cropped the outer edges of original satellite SIC frames to meet the spatial requirements of the deep learning model, which requires dimensions divisible by $2^3$ due to three pooling operations. The outcropping does not affect SIC areas. Here, SIPNet predicts the following 8 weeks using SIC data from the prior 8 weeks at each training iteration. The number of layers in the CNN is indicated in Supplementary Fig. 1, where, for example, $304 \times 320 \times 32$ corresponds to the sea ice data's spatial dimensions ($304 \times 320$) and the number of layers (32).

We used bootstrap SICs from the National Snow and Ice Data Center (NSIDC)[53], for model training and skill assessment. The dataset, derived from passive microwave radiometers, features a spatial resolution of 25 km. Our dataset spans from 1979 to 2022. Each sample was created by pairing an 8-week SIC segment as input with the subsequent 8-week SIC as target truth, using a 1-week step to generate samples across the time series. The samples were then randomly shuffled, with 5/6 allocated to the training set and 1/6 to the validation set, ensuring both sets comprehensively cover the study period. This study explores how ENSO affects Antarctic sea ice predictability, rather than focusing solely on model skill. To encompass a broader range of ENSO events, we hindcasted SIC from 1980 to 2022 with 1–8 week leads after the model is fully constructed. For instance, sea ice data from weeks 1–8 were employed as inputs to predicted SIC for weeks 9–16, with the 9th week representing a 1-week lead and the 16th week representing an 8-week lead. This process was repeated for weeks 2–9 to forecast weeks 10–17, iteratively generating all predictions. Based on the years of ENSO events, we extract the corresponding observed and predicted SICs and calculate the model's prediction skill under different ENSO phases to

analyze ENSO's impact on sea ice predictability, ensuring that the SIPNet model configuration remains consistent across all ENSO phases.

### Linear SIPNet model

The linear SIPNet model is achieved by deactivating all nonlinear activation functions within the SIPNet model (Supplementary Fig. 1b), while other parameter settings remain consistent with the SIPNet model. The linear SIPNet learns the linear processes from the entire training set and makes predictions for the target sea ice based on the initial time series, enabling the examination of Antarctic sea ice's linear predictability. The nonlinear and linear processes involved in sea ice evolution are built into SIPNet. Nonlinear SIPNet skill is evaluated using two approaches. The primary approach calculates it as the difference between total SIPNet skill and linear SIPNet skill, reflecting the contribution of nonlinear processes. If SIPNet outperforms linear SIPNet, it is because it incorporates nonlinear processes in addition to linear ones. The second approach is derived from nonlinear SIC predictions, which are obtained by subtracting linear SIPNet SIC predictions from total SIPNet SIC predictions. This study primarily employs the first method, with the second serving as supplementary validation.

### Linear Markov model

The Markov model here operates within the empirical orthogonal function (EOF) space, with its spatial structure determined by EOF eigenvectors, which are computed from weekly SIC anomalies from 1979 to 2022. The model's temporal dynamics follow a Markov process, where the transition functions are defined by the corresponding principal components. Specifically, the SIC anomalies, denoted as **V**, are decomposed into eigenvectors (**E**) and principal components (**P**) using the following relationship:

$$\boldsymbol{V} = \boldsymbol{E}\boldsymbol{P}^T \tag{2}$$

where the columns of **E** are orthogonal and the columns of **P** are orthonormal. T represents the matrix transpose. We truncated Eq. (2) to retain only the leading modes, based on the model's sensitivity to skill and error. The transition matrix (**A**) is calculated via a single-step correlation matrix, given by:

$$\boldsymbol{P}_{i+1} = \boldsymbol{A}\boldsymbol{P}_i + e_i \tag{3}$$

where $i$ represents the calendar week and $e_i$ is the model fit error. Multiplying both sides of this equation by $\mathbf{P}_i^T$ yields:

$$\boldsymbol{P}_{i+1}\boldsymbol{P}_i^T = \boldsymbol{A}\boldsymbol{P}_i\boldsymbol{P}_i^T + e_i\boldsymbol{P}_i^T \tag{4}$$

For optimal model fit, $e_i$ and $\boldsymbol{P}_i^T$ should be uncorrelated, leading to the transition matrix:

$$\boldsymbol{A} = (\boldsymbol{P}_{i+1}\boldsymbol{P}_i^T)(\boldsymbol{P}_i\boldsymbol{P}_i^T)^{-1} \tag{5}$$

This approach is applied to 52 subsets of P to compute the transition matrices corresponding to each calendar week.

To optimize the mode configuration for the Markov model, we conducted experiments to assess prediction skill and sensitivity by varying the number of retained leading modes. The results indicated that retaining seven leading SIC modes produced the best overall performance.

### Anomaly persistence model

Anomaly persistence forecast serves as the benchmark for assessing sea ice prediction skill. By assuming that historical anomaly will persist within defined time frames, anomaly persistence forecast uses the observed sea ice anomaly at the initial time as the ice anomaly in the target time. Autocorrelation coefficients between the initial and target states measure their skill. Although the autocorrelation between initial and target SIC anomalies is likely influenced by the existence of both linear and nonlinear processes, it mainly reflects the contribution of linear processes to sea ice predictability due to its nature of linear calculation. Weekly sea ice anomalies from 1979 to 2022 are generated by subtracting climatologies of the same period from the weekly SIC time series.

### SVD analysis

The interrelationship between Antarctic weekly SIC and global SST is explored using the singular value decomposition (SVD) analysis. This method facilitates the detection of coupled variability within the two variables. Singular vectors represent the spatial patterns of each variable, while the temporal variability is captured by projecting these spatial patterns onto the original time series. The primary SVD mode is designed to maximize covariance between the two variables. Consequently, the method reveals modes exhibiting both spatial and temporal patterns that dominate the variability in SIC and SST, which are strongly correlated with one another.

### The definition of ENSO events

The Niño 3.4 index[54] from the National Oceanic and Atmospheric Administration (NOAA) Physical Sciences Laboratory is employed for defining ENSO events from 1980 to 2022. ENSO events are identified using Niño 3.4 above 0.5, with a maximum above 1 from November to January of the following year. La Niña events are characterized by Niño 3.4 below −0.6, with a minimum below −1. Values between −0.55 and 0.55 indicate a neutral condition. There were 11 El Niño events, 10 La Niña events, and 11 neutral conditions throughout the study period.

### Model skill

Anomaly time series are generated by subtracting climatologies specific to each corresponding week from the weekly mean data. Model skill is measured by the anomaly correlation coefficient (ACC) between observations and predictions, as defined in Eq. (6):

$$\mathrm{ACC} = \frac{\sum_{i=1}^{n}(p_i - \bar{p})(g_i - \bar{g})}{\sqrt{\sum_{i=1}^{n}(p_i - \bar{p})^2}\sqrt{\sum_{i=1}^{n}(g_i - \bar{g})^2}} \tag{6}$$

where $p$ denotes the predicted SIC anomalies, $p_i$ denotes the SIC prediction anomaly at time $i$, $g$ denotes the observation anomalies. $n$ denotes the length of the time series. ACC calculations are confined to regions covered by sea ice.

In addition, previous research indicated that the strongest impact of ENSO on Antarctic sea ice occurs 6 months after ENSO matured in the tropic[13,17]. Thus, our analysis primarily focuses on sea ice predictability from March to August following ENSO events. The term "target week" denotes the predicted week, while "lead week" represents the number of weeks preceding the target week when the forecast was initiated.

### ACC histogram

Antarctic SIC observations were correlated with predictions at 1- to 6- week leads on a grid-by-grid basis, resulting in six sets of ACC maps representing SIPNet skill at 1- to 6- week lead times. These ACC values were then grouped by region and compiled into histograms to show their relative occurrence frequency across ACC values, which allow us to consolidate ACC changes as a function of its values. The histogram of ACC more effectively illustrates the shifts in ACC values among different regions, lead times, and models.

### Kolmogorov–Smirnov test

To assess the statistical significance of the differences between ACC distributions across various Antarctic regions, we employed the Kolmogorov–Smirnov (KS) test. The KS test is a non-parametric method to determine if two samples are drawn from the same distribution. We measured the significance of the observed differences by calculating the KS statistic and its $p$ value. A $p$ value below 0.05 signifies a statistically significant divergence in distributions.

## Data availability

The result data for this paper can be accessed on the figshare website (https://doi.org/10.6084/m9.figshare.24572866). Daily SICs from NSIDC are

available at https://doi.org/10.5067/7Q8HCCWS4I0R. The Niño3.4, Niño3, and Niño4 indices are provided at https://psl.noaa.gov/gcos_wgsp/Timeseries/. SST, SLP, SAT, and V at 850 hPa are from the latest European Centre for Medium-Range Weather Forecasts (ECMWF) reanalysis version 5 (ERA5), available at https://cds.climate.copernicus.eu/datasets/reanalysis-era5-single-levels?tab=download. The IOD index data is available at https://psl.noaa.gov/data/timeseries/month/data/dmi.had.long.data. The SAM index data is available at http://www.nerc-bas.ac.uk/icd/gjma/sam.html.

Received: 11 August 2024; Accepted: 13 February 2025;
Published online: 27 February 2025

## References

1. Bintanja, R., van Oldenborgh, G. J., Drijfhout, S. S., Wouters, B. & Katsman, C. A. Important role for ocean warming and increased ice-shelf melt in Antarctic sea-ice expansion. *Nat. Geosci.* **6**, 376–379 (2013).
2. Eayrs, C., Li, X., Raphael, M. N. & Holland, D. M. Rapid decline in Antarctic sea ice in recent years hints at future change. *Nat. Geosci.* **14**, 460–464 (2021).
3. Zhang, L. et al. The relative role of the subsurface Southern Ocean in driving negative Antarctic sea ice extent anomalies in 2016–2021. *Commun. Earth Environ.* **3**, 302 (2022).
4. Parkinson, C. L. A 40-y record reveals gradual Antarctic sea ice increases followed by decreases at rates far exceeding the rates seen in the Arctic. *Proc. Natl Acad. Sci. USA* **116**, 14414–14423 (2019).
5. Fogt, R. L., Sleinkofer, A. M., Raphael, M. N. & Handcock, M. S. A regime shift in seasonal total Antarctic sea ice extent in the twentieth century. *Nat. Clim. Change* **12**, 54–62 (2022).
6. Fetterer, F., Knowles, K., Meier, W. N., Savoie, M. & Windnagel, A. K. *Sea Ice Index. (G02135, Version 3)* [Data Set] (National Snow and Ice Data Center, 2017).
7. Purich, A. & Doddridge, E. W. Record low Antarctic sea ice coverage indicates a new sea ice state. *Commun. Earth Environ.* **4**, 314 (2023).
8. Chevallier, M., Massonnet, F., Goessling, H., Guémas, V. & Jung, T. Chapter 10—The role of sea ice in sub-seasonal predictability. In *Sub-Seasonal to Seasonal Prediction* (eds Robertson, A. W. & Vitart, F.) 201–221 (Elsevier, 2019).
9. Cai, W. et al. Changing El Niño–Southern Oscillation in a warming climate. *Nat. Rev. Earth Environ.* **2**, 628–644 (2021).
10. Turner, J. The El Niño–Southern Oscillation and Antarctica. *Int. J. Climatol.* **24**, 1–31 (2004).
11. Li, X. et al. Tropical teleconnection impacts on Antarctic climate changes. *Nat. Rev. Earth Environ.* **2**, 680–698 (2021).
12. Yuan, X., Kaplan, M. R. & Cane, M. A. The interconnected global climate system—a review of tropical–polar teleconnections. *J. Clim.* **31**, 5765–5792 (2018).
13. Yuan, X. & Martinson, D. G. Antarctic sea ice extent variability and its global connectivity. *J. Clim.* **13**, 1697–1717 (2000).
14. Yuan, X. & Martinson, D. G. The Antarctic dipole and its predictability. *Geophys. Res. Lett.* **28**, 3609–3612 (2001).
15. Liu, J., Yuan, X., Rind, D. & Martinson, D. G. Mechanism study of the ENSO and southern high latitude climate teleconnections. *Geophys. Res. Lett.* **29**, 24-21–24-24 (2002).
16. Wilson, A. B., Bromwich, D. H., Hines, K. M. & Wang, S.-H. El Niño flavors and their simulated impacts on atmospheric circulation in the high southern latitudes. *J. Clim.* **27**, 8934–8955 (2014).
17. Yuan, X. ENSO-related impacts on Antarctic sea ice: a synthesis of phenomenon and mechanisms. *Antarct. Sci.* **16**, 415–425 (2004).
18. Liu, J., Curry, J. A. & Martinson, D. G. Interpretation of recent Antarctic sea ice variability. *Geophys. Res. Lett.* **31**, L02205 (2004).
19. Bushuk, M. et al. Seasonal prediction and predictability of regional Antarctic sea ice. *J. Clim.* **34**, 6207–6233 (2021).
20. Morioka, Y., Doi, T., Iovino, D., Masina, S. & Behera, S. K. Role of sea-ice initialization in climate predictability over the Weddell Sea. *Sci. Rep.* **9**, 2457 (2019).
21. Marchi, S. et al. Reemergence of Antarctic sea ice predictability and its link to deep ocean mixing in global climate models. *Clim. Dyn.* **52**, 2775–2797 (2019).
22. Holland, M. M., Blanchard-Wrigglesworth, E., Kay, J. & Vavrus, S. Initial-value predictability of Antarctic sea ice in the Community Climate System Model 3. *Geophys. Res. Lett.* **40**, 2121–2124 (2013).
23. Libera, S., Hobbs, W., Klocker, A., Meyer, A. & Matear, R. Ocean-sea ice processes and their role in multi-month predictability of Antarctic sea ice. *Geophys. Res. Lett.* **49**, e2021GL097047 (2022).
24. Morioka, Y., Iovino, D., Cipollone, A., Masina, S. & Behera, S. Summertime sea-ice prediction in the Weddell Sea improved by sea-ice thickness initialization. *Sci. Rep.* **11**, 11475 (2021).
25. Ordonez, A. C., Bitz, C. M. & Blanchard-Wrigglesworth, E. Processes controlling Arctic and Antarctic sea ice predictability in the Community Earth System Model. *J. Clim.* **31**, 9771–9786 (2018).
26. Liu, Y. et al. Decadal oscillation provides skillful multiyear predictions of Antarctic sea ice. *Nat. Commun.* **14**, 8286–8286 (2023).
27. Meehl, G. A., Arblaster, J. M., Bitz, C. M., Chung, C. T. Y. & Teng, H. Antarctic sea-ice expansion between 2000 and 2014 driven by tropical Pacific decadal climate variability. *Nat. Geosci.* **9**, 590–595 (2016).
28. Himmich, K. et al. Drivers of Antarctic sea ice advance. *Nat. Commun.* **14**, 6219 (2023).
29. Rackow, T. et al. Delayed Antarctic sea-ice decline in high-resolution climate change simulations. *Nat. Commun.* **13**, 637 (2022).
30. Massonnet, F. et al. Assessment of summer 2019–2020 sea-ice forecasts for the Southern Ocean. Technical Note, Université catholique de Louvain available at https://fmassonn.github.io/sipnsouth.github.io/ (2022).
31. Zampieri, L., Goessling, H. F. & Jung, T. Predictability of Antarctic sea ice edge on subseasonal time scales. *Geophys. Res. Lett.* **46**, 9719–9727 (2019).
32. Shu, Q. et al. Assessment of sea ice extent in CMIP6 with comparison to observations and CMIP5. *Geophys. Res. Lett.* **47**, e2020GL087965 (2020).
33. Roach, L. A. et al. Antarctic sea ice area in CMIP6. *Geophys. Res. Lett.* **47**, e2019GL086729 (2020).
34. Wang, Y. et al. Reassessing seasonal sea ice predictability of the Pacific-Arctic sector using a Markov model. *Cryosphere* **16**, 1141–1156 (2022).
35. Wang, Y. et al. Subseasonal prediction of regional Antarctic sea ice by a deep learning model. *Geophys. Res. Lett.* **50**, e2023GL104347 (2023).
36. Flatau, M. & Kim, Y.-J. Interaction between the MJO and polar circulations. *J. Clim.* **26**, 3562–3574 (2013).
37. Ding, Q. & Steig, E. J. Temperature change on the Antarctic Peninsula linked to the tropical Pacific. *J. Clim.* **26**, 7570–7585 (2013).
38. Li, X., Holland, D. M., Gerber, E. P. & Yoo, C. Impacts of the north and tropical Atlantic Ocean on the Antarctic Peninsula and sea ice. *Nature* **505**, 538–542 (2014).
39. Goyal, R., Jucker, M., Gupta, A. S. & England, M. H. A New Zonal Wave-3 Index for the Southern Hemisphere. *J. Clim.* **35**, 5137–5149 (2022).
40. Eabry, M. D., Goyal, R., Taschetto, A. S., Hobbs, W. & Sen Gupta, A. Combined impacts of southern annular mode and Zonal Wave 3 on Antarctic sea ice variability. *J. Clim.* **37**, 1759–1775 (2024).
41. Lee, H.-J. & Seo, K.-H. Impact of the Madden-Julian oscillation on Antarctic sea ice and its dynamical mechanism. *Sci. Rep.* **9**, 10761 (2019).
42. Yuan, X. & Li, C. Climate modes in southern high latitudes and their impacts on Antarctic sea ice. *J. Geophys. Res. Oceans* **113**, C06S91 (2008).

43. Thompson, D. W. J. & Wallace, J. M. Annular modes in the extratropical circulation. Part I: month-to-month variability. *J. Clim.* **13**, 1000–1016 (2000).
44. Sun, D., Xue, F. & Zhou, T. Impacts of two types of El Niño on atmospheric circulation in the Southern Hemisphere. *Adv. Atmos. Sci.* **30**, 1732–1742 (2013).
45. Lee, T. et al. Record warming in the South Pacific and western Antarctica associated with the strong central-Pacific El Niño in 2009–10. *Geophys. Res. Lett.* **37**, L19704 (2010).
46. Ciasto, L. M., Simpkins, G. R. & England, M. H. Teleconnections between tropical Pacific SST anomalies and extratropical Southern Hemisphere climate. *J. Clim.* **28**, 56–65 (2015).
47. Zhang, C., Li, T. & Li, S. Impacts of CP and EP El Nino events on the Antarctic sea ice in Austral Spring. *J. Clim.* **34**, 9327–9348 (2021).
48. Ren, H.-L. & Jin, F.-F. Niño indices for two types of ENSO. *Geophys. Res. Lett.* **38**, L04704 (2011).
49. Nuncio, M. & Yuan, X. The influence of the Indian Ocean Dipole on Antarctic sea ice. *J. Clim.* **28**, 2682–2690 (2014).
50. Ren, Y. & Li, X. Predicting the daily sea ice concentration on a subseasonal scale of the Pan-Arctic during the melting season by a deep learning model. *IEEE Trans. Geosci. Remote Sens.* **61**, 4301315 (2023).
51. Ren, Y., Li, X. & Zhang, W. A data-driven deep learning model for weekly sea ice concentration prediction of the Pan-Arctic during the melting season. *IEEE Trans. Geosci. Remote Sens.* **60**, 4304819 (2022).
52. He, K., Zhang, X., Ren, S. & Sun, J. Identity mappings in deep residual networks. In *Computer Vision – ECCV 2016*. (eds Leibe, B., Matas, J., Sebe, N. & Welling, M.) Vol 9908. Lecture Notes in Computer Science. https://doi.org/10.1007/978-3-319-46493-0_38 (Springer, Cham., 2016).
53. Comiso, J. C. *Bootstrap Sea Ice Concentrations from Nimbus-7 SMMR and DMSP SSM/I-SSMIS, Version 3* (NASA National Snow and Ice Data Center Distributed Active Archive Center, 2017).
54. Rayner, N. A. et al. Global analyses of sea surface temperature, sea ice, and night marine air temperature since the late nineteenth century. *J. Geophys. Res. Atmos.* **108**, 1063–1082 (2003).


## Acknowledgements

This work is funded by the National Natural Science Foundation of China (42106223); Natural Science Foundation of Shandong Province, China (ZR2021QD059), and Laoshan Laboratory (LSKJ202202303). X.Y. receives support from the Lamont-Doherty Earth Observatory of Columbia University. We also thank Jianna Martinez from Columbia University for contributing to the idea development of this manuscript.

## Author contributions

Y.W., X.Y., and X.L. conceived this study. Y.W. and Y.R. developed the methodology and Y.W. and X.Y. conducted and analyzed the experiments. All authors discussed the results and wrote the manuscript together.

## Competing interests

The authors declare no competing interests.

## Additional information

**Supplementary information** The online version contains supplementary material available at https://doi.org/10.1038/s41612-025-00962-9.

**Correspondence** and requests for materials should be addressed to Xiaojun Yuan or Xiaofeng Li.